

Potential Utility of Spectral Angle Mapper and Spectral Information Divergence Methods for mapping lower Vindhyan Rocks and Their Accuracy Assessment with Respect to Conventional Lithological Map in Jharkhand, India

D. Ananth Rao¹ · Arindam Guha²

Received: 4 March 2016 / Accepted: 4 December 2017 / Published online: 10 January 2018
© Indian Society of Remote Sensing 2018

Abstract

In this study, we have evaluated the potential use of spectral mapping algorithms in deriving spectrolithological maps of metasedimentary rocks of Vindhyan group of rocks. In this regard, we have processed visible near infrared (VNIR) and shortwave infrared (SWIR) bands of Advanced Spaceborne Thermal Emission and Reflection Radiometer (ASTER) data using similarity based spectral mapping algorithms such as spectral angle mapper (SAM) and spectral information divergence (SID). Laboratory spectra were collected by Fieldspec 3© spectroradiometer for main rock types of study area and the spectra were resampled to ASTER bandwidth to compare laboratory spectra with image spectra of respective rocks. Overall matching of image spectra of rocks with their ASTER resampled laboratory counterparts justified the spectral integrity of these rocks on the image. Therefore, image spectra of rocks were used as end member for deriving spectral maps using SAM and SID method. These maps were compared with the conventional field based lithological map (consequently updated using ASTER false colour image composite and band ratio images). SAM spectral map had over all accuracy of 67.41% and the SID map had overall accuracy of 69.67%. Present study has brought out the fact that spectral mapping algorithms would be useful in deriving moderate accuracy lithological maps even if the sedimentary rocks are of close mineralogy and these rocks have very close reflectance spectra within the spectral bandwidth of ASTER sensor. Spectral maps corroborate well with the discrete geochemical data.

Keywords Confusion matrix · Spectral angle mapper · Spectral information divergence · Spectral absorption feature · Sedimentary rocks · Vindhyan group of rocks

Introduction

Spaceborne remote sensors have an advantage for their synoptic viewing capability on capturing information for reasonably large areas at a time. This was proved advantageous for spatial mapping of rock types of different geological provenances since the launch of LANDSAT

programs by National Aeronautics Space Administration (NASA), America (Bhan and Hegde 1985; Meer Van Der et al. 2012; Sabins 1999). Broad spectral bands of Landsat Enhanced Thematic Mapper (ETM) were used for mapping of rock types of different sedimentary rocks for containing spectrally sensitive iron, clay and carbonate minerals (Andrews Deller 2006; Dogan 2008; Kavak 2005; Leverington 2010; Mezned et al. 2010; Tangestani and Moore 2000; White et al. 1997). Remote sensing sensors actually collect spectral radiances in few spectral bands. These spectral radiances data are further calibrated to reflectance or emittance for delineating terrain elements and also used for deriving band rationing and spectral indices. Accuracies of these information are dependent on sensor parameters such as spectral resolution (number of spectral bands used

✉ D. Ananth Rao
ananthgeo3@gmail.com

Arindam Guha
arindamisro@gmail.com

¹ Central Ground Water Board, Chandigarh, India

² National Remote Sensing Centre, Indian Space Research Organisation, Balanagar 500037, India

for collecting spectral information), temporal resolution (frequency or interval of data collection), spatial resolution (area of minimum detectable unit on the ground) of data, radiometric details or degree of quantization with which spectral information's are collected. In this regard, band ratio images have also been coined for delineating different rock types using Landsat Thematic Mapper (TM), ETM based bands (Bhan and Hegde 1985; Sabins 1999).

In last two decades, we have witnessed the launch and extensive utilization of advanced multispectral sensor known as Advanced Space borne Thermal Emission and Reflection radiometer (ASTER); which can collect information with reasonably significant spectral details coupled with its moderate spatial resolution and appreciable radiometric resolution. In this regard, it is also important to mention that the capability of hyperspectral spaceborne sensors (sensors collect continuous and contiguous spectral data in finer spectral bandwidth); which can collect image with spectral information comparable with the laboratory spectra. Hyperion, global hyperspectral sensor, which collect information with 10 nm spectral resolution and 30 m spatial resolution is operative within visible near Infrared and shortwave infrared (VNIR–SWIR) spectral domain. Although, spaceborne hyperspectral sensors have its potentials for lithological mapping, but limited swath, coarser spatial resolution, poor signal to noise ratio (SNR) and intrinsic optical distortions of these sensors (Smile effect etc.) limit the prospect of hyperspectral sensors for lithological mapping with higher accuracy than their airborne counterparts (Kruse et al. 2003a; b; San and Lutfi Suzen 2011). On other hand, multispectral sensors collect spectral data in few significant spectral bands with larger swath, better SNR and higher spatial resolution (Chabrilat et al. 2000; Chen et al. 2010). ASTER sensor with nine spectral bands in VNIR and SWIR domain and five spectral bands in thermal infrared (TIR) region have provided geologist, the scope of using spectral remote sensing data for mapping different rock types. Recent literatures of geological remote sensing have brought out wide geological research applications using ASTER data (Hewson et al. 2005; Hubbard and Crowley 2005; Rowan and Mars 2003; Rowan et al. 2006; Tangestani et al. 2011; Tommasao and Rubinstein 2007). Detail records of different spectral indices for mapping different silicate rocks using ASTER data are also available in the literature (Kalinowski and Oliver 2004). It was also shown that ASTER data could delineate carbonate, hydroxyl mineral bearing and iron mineral rocks effectively and derived similar accuracy in lithological mapping with reference to Hyperion data (Pour and Hashim 2014). Further, it was demonstrated that the classification accuracy of lithological maps derived from ASTER and Hyperion data were similar to each other in terms of overall accuracy and Kappa coefficient (Zhang et al. 2007). However, records of ASTER

data utilization for mapping of sedimentary rocks exposed under tropical weathering set up are limited. ASTER data were subjected to spectral mapping of different volcanic rocks in Iran and the accuracy of spectral maps were tested for selected ground truth areas without including entire area using conventional lithological map (Hadigheh and Ranjbar 2013). Efficiency of spectral angle mapper method was tested on ASTER data and results of the mapping was validated with reference to the image enhanced products like principle component image composite and band ratio images for different volcanoclastic and pyroclastic rocks in Golova region (Gürsoy and Kaya 2017). In recent time, it was demonstrated that conventional image enhancement techniques such different band combinations, FCC image of principle component were suitable for mapping pre-rift and syn rift sedimentary units in Egypt (Youssef et al. 2009). But, Implementation of spectral mapping algorithm for mapping sedimentary rocks is a challenge as these rocks are often known for contrasting textures (grain size varies one rock to another) but close mineralogy (e.g. Greywacke and mudstone are compositionally close). Further, mineralogical variations within a specific sedimentary unit are gradational. Sedimentary rocks are easily weathered and often have poorly preserved exposures in patches under the tropical weathering set up and chemical weathering (oxidation and hydration). This often contributes in changing the surface mineralogy of these rocks. Therefore, in this study, attempt has been made to use ASTER data for lithological mapping based on the implementation of two important similarly based spectral mapping algorithms. These algorithms take into consideration overall shape of end member spectra and their contrast rather focusing on diagnostic absorption feature. These similarity based algorithms are expected to derive good results when spectra of different rocks have closely spaced absorption features in wavelength domain. We have used spectral profiles of sedimentary rocks of lower Vindhyan Group collected from ASTER image and these image spectra are compared with the laboratory spectra of same rock types after resampling them to the bandwidth of ASTER channels. Once the image spectra and respective laboratory spectra of each rock type are compared and proved similar, these image spectra are used in spectral mapping algorithms and spectral maps thus prepared have been compared with the geological map prepared using field survey and supplemented with image interpretation of ASTER data.

Study Area and General Geology

The study area is bounded by latitude 24°23'33" to 24°28'04" and longitude from 83°32'15" to 83°37'40" (Fig. 1). The study area is situated in North East part of

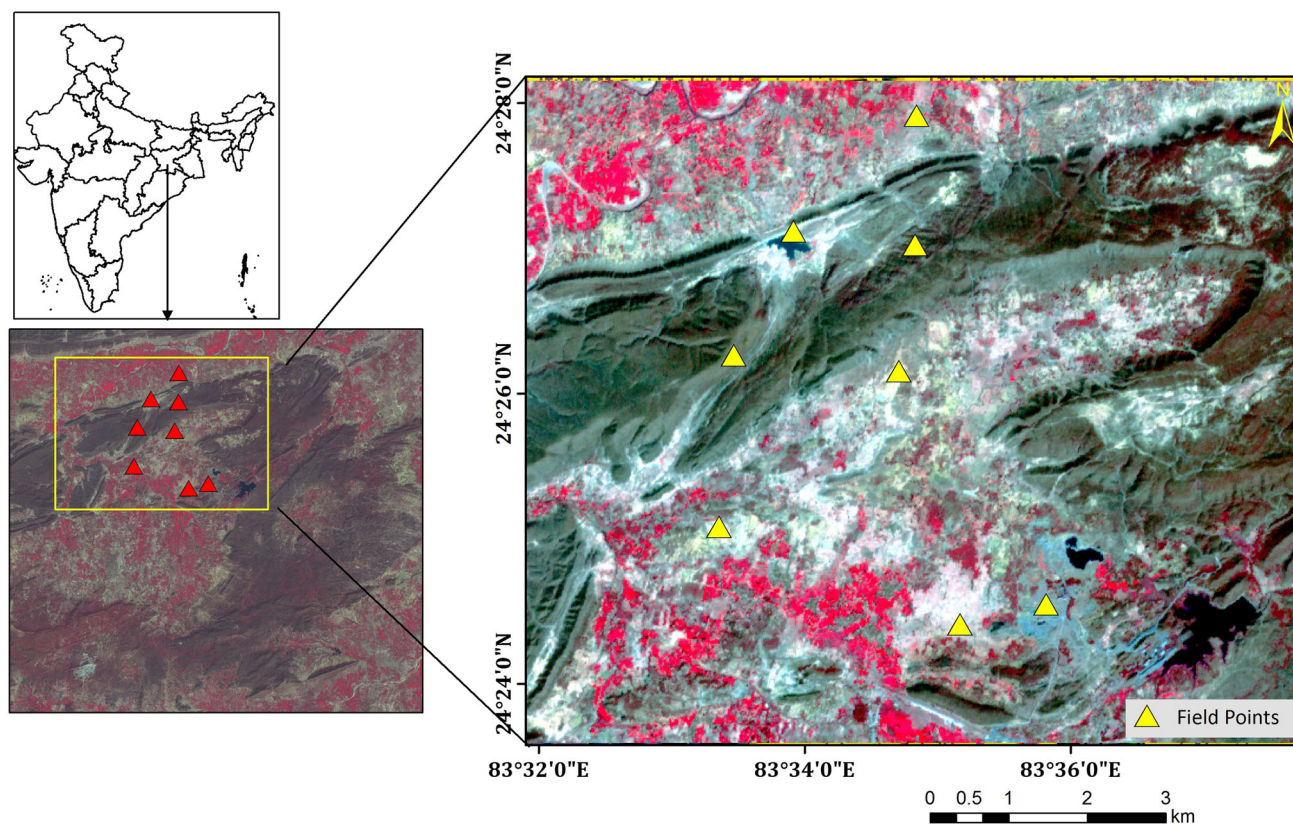


Fig. 1 Study area shown with the field points on the ASTER FCC (false colour composite) image. R = 3rd band G = 2nd band B = 1st band). Field points are the place from where samples were collected for spectral analysis (color figure online)

Palamu and Garhwa districts, Jharkhand state, India and Vindhyan metasediments of Proterozoic age. The Vindhyan rocks were deposited in intra cratonic basin in Proterozoic time. Rocks exposed in the study area are stratigraphically related to lower part of Vindhyan groups; which were deposited under marine environment prevailed during the initial period of basin formation (Valdiya 2010). In the study area, limestone for lower basal formation and Khenjua formation (occur along fold limb) were mapped. Limestone of Bhawanthapur and sandstone at south west of Duwarasai area were shown in the Fig. 2. Bhawanthapur area is known as for the important limestone mine.

Materials and Methods

Data

We used VNIR–SWIR bands of ASTER data for the purpose of present study. The detail specification of ASTER datasets used for spectral mapping provided in Table 1 (Abrams 2000). We also used the regional geological map of the study area, prepared by Geological Survey of India (1:50,000) (GSI, Unpublished) (Fig. 3). We have updated

the reference geological map using the field data collected along selected traverses and also using the ASTER false colour composite (FCC) based on image interpretation. In addition to above, spectral profiles of rocks were collected in the laboratory used as a reference. Spectral data were collected using Fieldspec 3© spectro radiometer and halogen lamp was used as illuminator. This spectrometer is operative within the spectral domain of 350–2500 nm.

Methods

The entire methodology has been segmented in six parts; each segment is elaborated in separate sub-sections. These segments are 1. ASTER data preprocessing and coregistration of geological map (reference) with ASTER data, 2. Reference geological map updation, 3. Spectral data collection and end member selection, 4. Spectral mapping, 5. Accuracy assessment, 6. Point geochemical data collection and analysis to relate them with spectral map. A flow chart (Fig. 3) is also provided to illustrate the links between major sequences of the methods followed for spectral mapping.

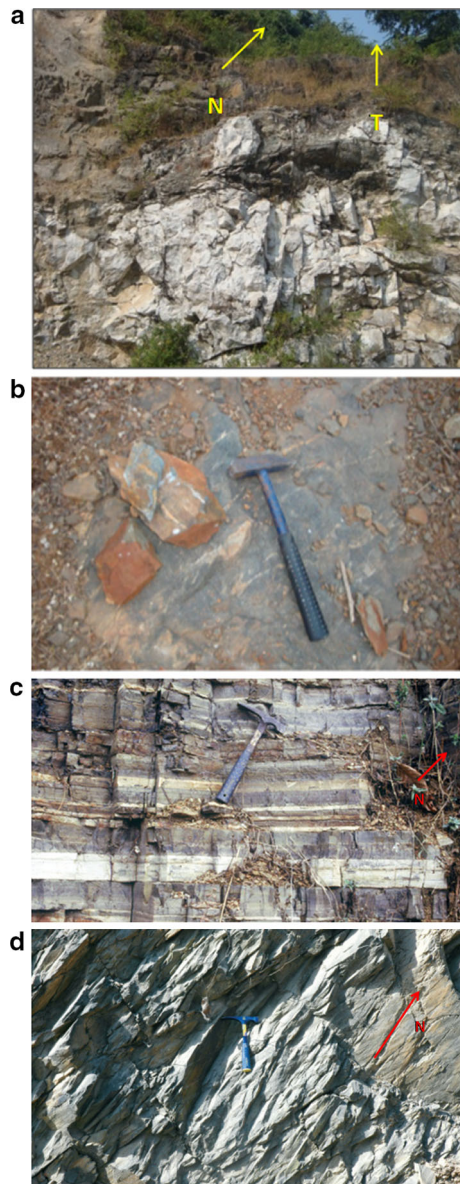


Fig. 2 **a** Limestone near Bhawanthiput section (N = NORTH). **b** Surface exposure Sandstone at southwest of Duwarsi. **c** Porcellanite at the Baligarh area (North West part of the study area). **d** Shale exposed near Sindhuria village (south-eastpart of the study area). Top of the field photos can be understood from the top of the hammer or following the arrow written with “T”. North direction is shown with arrow and label “N”

Preparation of Reference Geological Map

Field work was carried out along selected traverses to collect rock samples and also to update existing geological map. The geological map (1:50,000 scale) was further modified based on field survey and image interpretation of ASTER false colour composite image at few places (Fig. 2). Porcellanite (P) had widely distributed exposures in the study area (Fig. 4a). It was delineated in the ASTER

FCC image from other rocks based on its bright greenish tone. Sandstone (S) exposures were delineated from porcellanite based on its relatively rough texture (i.e. fractured) with the reddish green in the false color composite (Fig. 4a). Shale was characterized with blush tint in the same FCC image. Limestone exposures had brighter tone and exposures were found in the low lying areas and characterized with the occurrence of sparse vegetation than the calcareous shale (Fig. 4a). In the band ratio image derived using band 6, band 9 and band 8 of ASTER sensor, limestone was brighter than porcellanite (Fig. 4b). The updated geological map derived from image interpretation of ASTER FCC image is illustrated in Fig. 4c.

Preparation of Reference Spectral Database and Spectral Endmember Selection

Field work was carried out to collect the rock samples for acquiring spectral profiles and also updating the existing geological map of the study area. Rock samples were cut into rectangular chips (size ranges from 5" × 7" to 6" × 7") for collecting the rock spectra. Spectral profiles of rocks were collected using the Fieldspec 3© spectroradiometer using halogen as light source in the laboratory condition (Fig. 4a). The field of view used for collecting the spectral profiles was 25° and angle between the source of light and measurement sensor was kept 45° (this angle is called phase angle). The approach and methodology followed for collecting rock spectra have already been discussed in the published literatures (Milton et al. 2009; Guha et al. 2012a, b, 2013). Feature at 0.6 μm in addition to prominent absorption feature at 2.33 μm (Fig. 5).

Further, these laboratory spectral profiles of rocks were resampled to ASTER VNIR–SWIR bandwidth (Fig. 4b). It was observed from the analysis of each end member spectra that porcellanite and sandstone had their diagnostic absorption feature in VNIR bands around 0.8 and 0.6 μm respectively. On the other hand, sandstone was characterized with two absorption features in 2.2 and 2.33 μm in SWIR domain whereas porcellanite was identified with one absorption feature at 2.33 μm. Limestone had absorption at 2.33 μm in its reflectance spectra. Calcareous shale with Fe concretion was identified with absorption

Spectral integrity of ASTER derived image spectra of selected rock exposures of Porcellanite and limestone were checked based on comparing them with their respective ASTER resampled counterparts (Fig. 6a, b). It was found that spectral profiles of these rocks were well translated from sample to image and the overall shape of ASTER resampled laboratory spectra matches well with their image spectra counterpart (Fig. 6a, b). Therefore a mean image spectrum (mean spectra of different pixels of same rock) of each rock was used as end member for spectral mapping.

Table 1 ASTER data specifications

Data product aster L1A	Spectral bands	Spectral range (μm)	Spatial resolution (m)	Radiometric resolution (in terms of bits)
VNIR	1	0.5–0.60	15	8
	2	0.63–0.69	15	8
	3 N	0.78–0.86	15	8
	3B	0.78–0.86	15	8
SWIR	4	1.60–1.70	30	8
	5	2.145–2.185	30	8
	6	2.185–2.225	30	8
	7	2.235–2.285	30	8
	8	2.295–2.365	30	8
	9	2.360–2.430	30	8

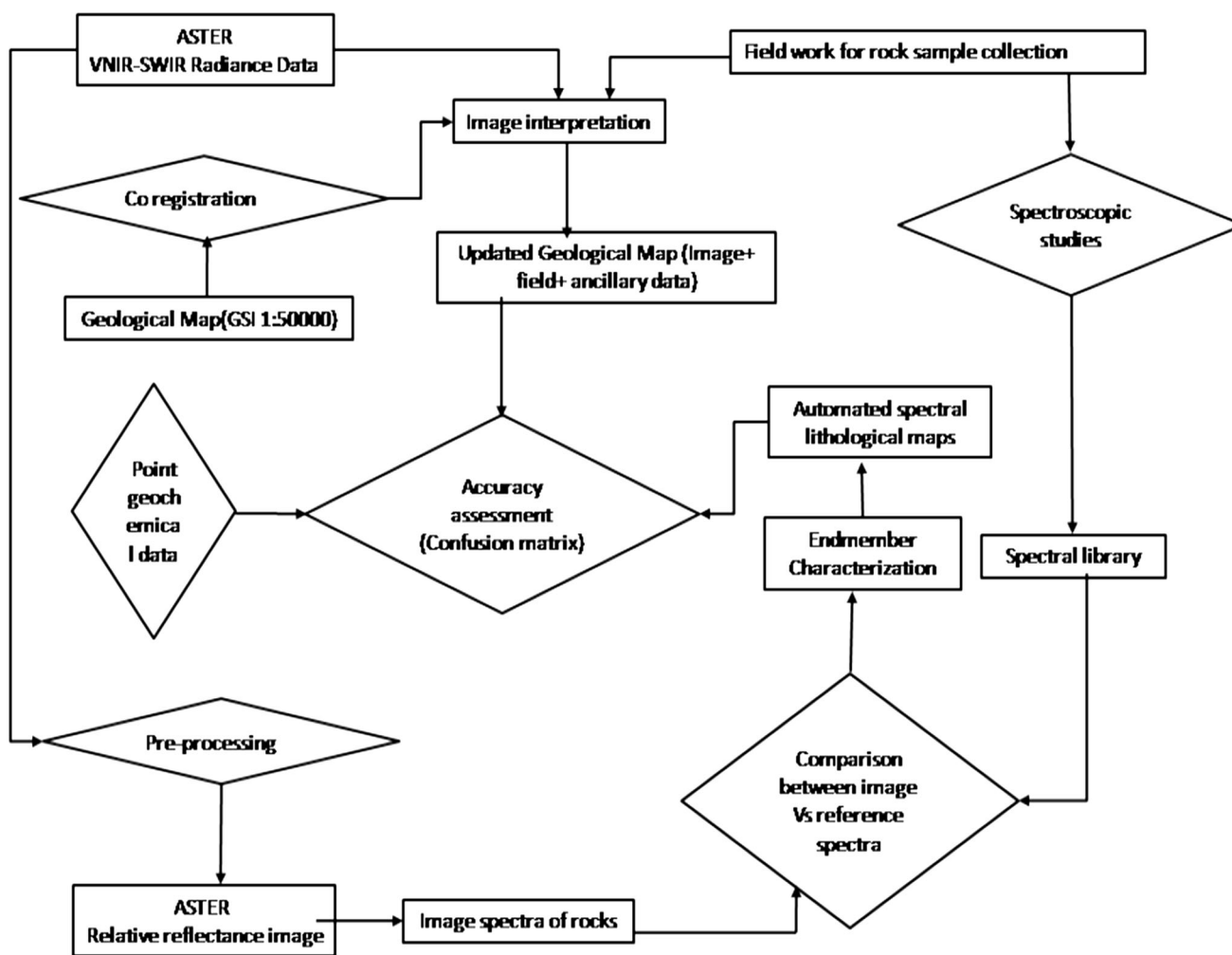


Fig. 3 Flowchart showing details of the methodology

Selection of image spectra provides the scope for incorporating the spectral variability of each rock across the spatial domain of their occurrence. For implementing

spectral mapping algorithms, mean image spectra of each lithounits collected from the few region of interest (ROI) from the prominent exposures of the rocks.

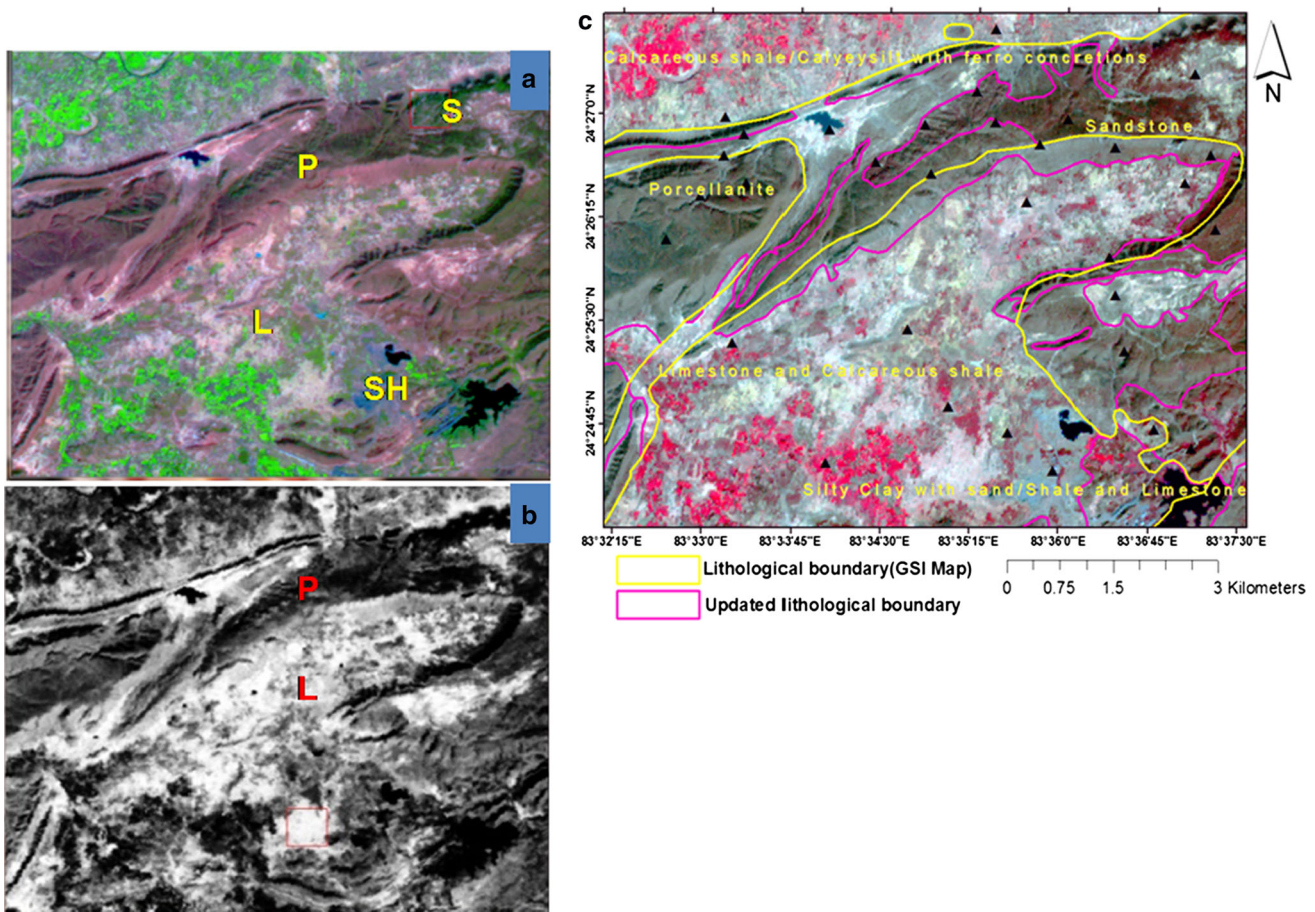


Fig. 4 **a** False colour composite of ASTER image delineating major rock types (In this FCC, Red = Band 4, Green = Band 3 and Blue = Band 1 of ASER). Band ratio (band 6 + band band 9) band 8

Aster Data Preprocessing

ASTER level 1B data was used for mapping lithology of the area. At first, ASTER level 1B data were preprocessed to derive reflectance image. VNIR bands of ASTER data were calibrated using IARR (Internal Average Relative Reflectance) method; whereas SWIR bands were calibrated using Log residual method (ITT 2014). Both the methods are “in-scene atmospheric correction” method. Calibration was done for deriving relative reflectance from radiance data (ASTER level 1B data is georectified radiance data). The IARR method was used (this method uses mean radiance of all the terrain element as a normalizing factor) for deriving relative reflectance of VNIR bands, whereas log residual (LR) method was used for SWIR bands (Azizi et al. 2010). The log residual method by normalizing the radiance to calculate geometric mean for each pixel to eliminate effect of topography consequently spatial mean of radiance of all pixels for each band was used to normalize radiance of each pixels of particular band to derive relative reflectance (ITT 2014). Once, relative reflectance

used to show the spectral contrast between two mineralogically similar rocks. L, limestone; P, porcellanite; SH, shale and S, sandstone (color figure online)

image was derived, vegetation covers were masked in ASTER data using the NDVI image derived using 3rd and 2nd band of ASTER data. NDVI greater than 0.5 values were used as cut off to mask vegetation covers.

Aster Data Processing and Spectral Mapping

For spatial mapping of rocks using spectral characters, we used spectral mapping algorithms known as spectral angle mapper (SAM) and spectral information divergence (SID). In SAM method, spectra of reference and pixel of the image were considered as vectors and consequently angle (SAM angle) between these two vectors in that data dimension space were calculated to measure the spectral similarity (Chen et al. 2010). In this method, similarity of reference and pixel spectra was compared based on SAM angle. As per this method, smaller the SAM angle, better would be the match/similarity between the target and the pixel spectra. SAM algorithm was found suitable for separating targets based on overall shape of the spectra rather than the specific absorption features (Chen et al. 2010).

Fig. 5 Reflectance spectra of type samples of different rocks of the study area collected using Fieldspec 3 spectrometer. **b** ASTER resampled counterpart of laboratory reflectance spectra

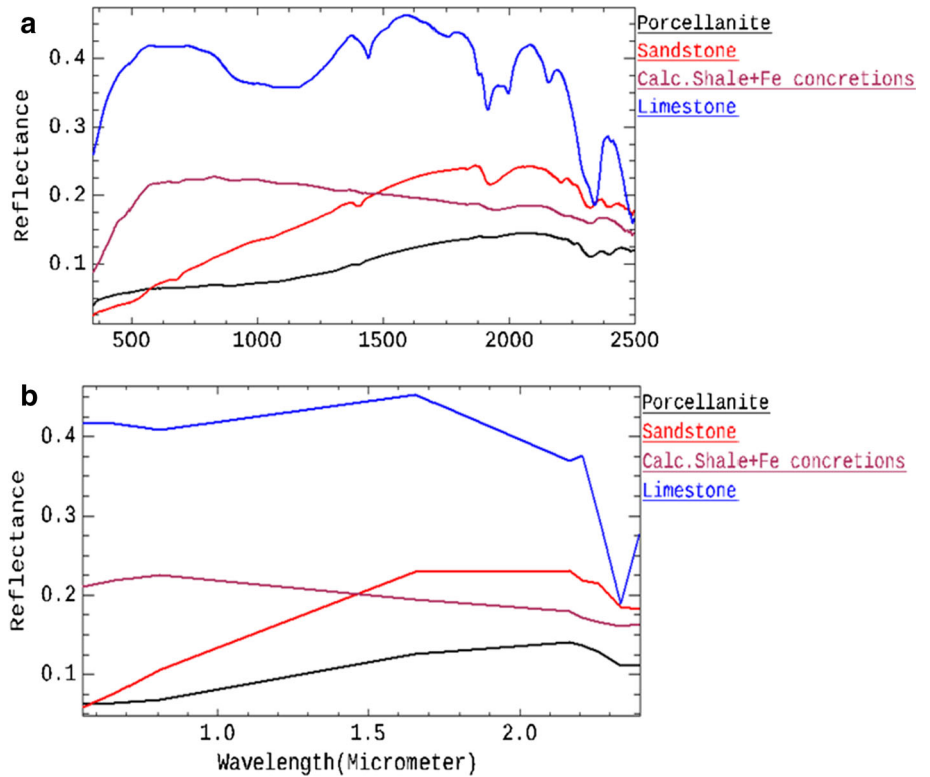
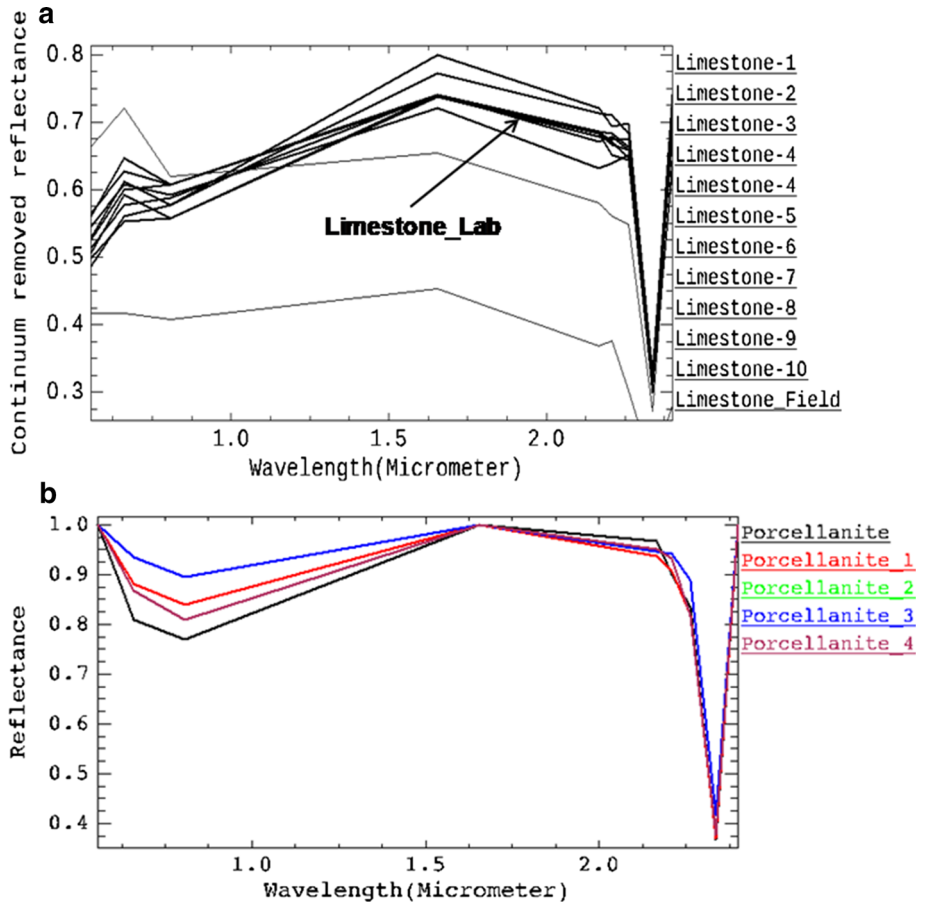


Fig. 6 a Image spectrum of each of the limestone type sample is compared with corresponding ASTER convolved laboratory spectra. Limestone, **b** image spectrum of each of the limestone type sample is compared with corresponding ASTER convolved laboratory spectra



SID was also used along with spectral angle mapper (SAM) for spatial mapping of rock types. SID algorithm calculates statistical divergence to derive the similarity between reference end member spectra and pixel spectra (Chang 1999). SID algorithm assumes the spectral feature of mixed pixel is a random variable and spectral histogram was used to determine the shape of probability density function (Chang 1999). The spectral similarity between target and reference was measured based on the contrast or differences in the probabilistic behavior between the target and sensor (Chang 1999). This method was known effective in using spectral correlation between target and reference as the key for target delineation. SAM is regarded deterministic method while SID is probabilistic methods as it could accommodate specified tolerance in the spectral variations of target for spectral delineation in the scale of 0–1 (Chang 1999). SAM and SID were used to derive the lithological maps (Fig. 7b, c.).

Accuracy Assessment

We used confusion matrix analysis as statistical comparison method of accuracy assessment of automated spectral maps of rock types with the reference lithological map derived from field survey and image interpretation (Congalton 1991). Confusion matrix was used to find out the accuracy of spatial distribution of each rock type in each of the spectral map with respect to the same lithological map.

Based on matrix based analysis, parameters like overall accuracy, producer accuracy, user accuracy, error of omission, error of commission were estimated.

Wet Chemical Analysis

We have taken samples from selected points to relate the spectral map with the broad variation of silica and calcium carbonate. The rocks of the study area are known for varying calcium carbonate concentration and silica variation. For example, calcium carbonate gradually decreases from limestone to Porcellanite to shale while silica is expected to increase.

We have carried out simplistic wet chemical analysis of the samples (IBM 2017). In this method, each of the rock samples were crushed and sieved into 3–5 mm size. Then 100 g of sample were prepared for each rock after mechanically grinding it and sieving it. The powdered sample finally was used for chemical analysis. 500 mg of powdered sample was taken in a beaker and 25 ml 1:1 Hydrochloric acid was added with it. Then the sample is dried on hot plate at 250–300 °C for an hour. After this, 5 ml concentrated Hydrochloric acid and 50 ml distilled water were added to it and boiled on hot plate at 250 °C. After boiling, the solution was filtered and further it was collected in 250 ml volumetric flask for estimating CaO, SiO₂ etc. CaCO₃ was derived from CaO values assuming entire CaO was combined with CaO (Table 2).

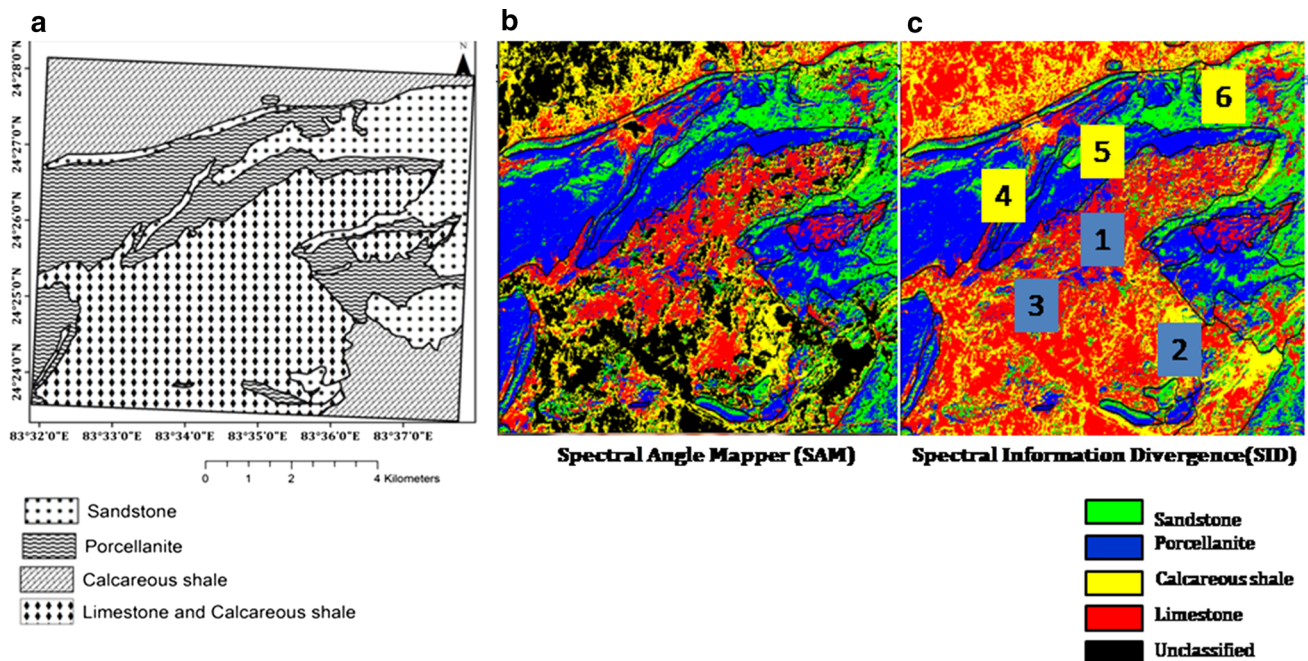


Fig. 7 a Updated lithological map derived based on ASTER FCC image interpretation and limited field traverses. b Lithological map derived using spectral angle mapper (SAM) algorithm. c. Lithological map derived using spectral information divergence (SID) algorithm

Table 2 Statistical comparison of SAM and reference lithological map

Lithounits/rock types	Producer's accuracy (in %)	User accuracy (in %)	Commission (%)	Omission (%)
<i>Accuracy assessment</i>				
Limestone	60.11	83.66	16.28	41.47
Sandstone	58.09	67.89	32.46	42.16
Porcellanite	84.48	78.43	23.59	15.55
Calc. shale with Fe concretions	61.45	50.30	49.37	38.51

Overall accuracy = (104,480/154,971) = 67.4191%; Kappa coefficient = 0.5583

Results and discussions

SAM and SID derived lithological maps had moderate overall accuracy with respect to reference geological map. SAM map had accuracy 67.41% (Table 3) whereas SID map had over all accuracy 69.67% (Fig. 7b and c and Table 3). It was also observed that SID map reflected overall accuracy slightly higher in comparison to the SAM map. This was due to the fact that the SAM was deterministic algorithm and it accommodated lesser variability in the pixel spectra (with respect to end member spectra) during classification than SID, which was probabilistic algorithm (Chang 1999). However, both the algorithms were conceived assuming pixel spectra as vector to highlight overall spectral variations (Chang 1999). These algorithms performs well in delineating sedimentary units which can be mapped based on the overall spectral contrast within the bandwidth of ASTER data in contrary to using diagnostic spectral feature based spectral mapping. However, lower spectral contrast of the rocks within the bandwidth of ASTER data was responsible for reduced accuracy (around 70%) for these spectral maps. Lower spectra contrast of spectral characters of these rock types was attributed to weathering, in situ land cover developed above the rocks and intra-pixel mixing of different rocks resulted due to their gradational facies variations and also for the coarser pixel size of ASTER than the size of the preserved exposures. Moreover, while preparing reference geological map during field survey, it was possible to

integrate the geoscientific knowledge on geological trend of the exposures, field evidences from geological sections of river, channel, to extrapolate the boundary of different rock types beyond the extent of surface exposures (Fig. 7a). On the other hand, spectral map was derived here based on spectral signature of pixels from the surface rock exposures. In addition, physical absence of exposure was another limiting factor for such mapping. Therefore, accuracy of spectral map on lithology was also controlled by the extent to which rocks were weathered, type of land cover developed above each rock type and the distinctiveness of the spectral feature of rock types. It was observed that calcareous shale were poorly classified in both the spectral maps as error of omission and error of commission both were higher for calcareous shale. This was due to fact that calcareous shale was spectrally similar with limestone and known for few surface exposures (Tables 2, 3). This had reduced low producer accuracy for calcareous shale in comparison to limestone and porcellanite having relatively large exposures and intense absorption features in their respective reflectance spectra (Tables 2, 3).

Calcium carbonate variations in the samples occurring within limestone (1, 2 sample location in Fig. 7c) was higher than the calcium carbonate concentration in shale (2) and porcellanite (4, 5). Silica content was higher in sample occurring within sandstone (6) (Fig. 7c and Table 4).

Table 3 Statistical comparison of SID and reference lithological map

Lithounits/rock types	Producer's accuracy (in %)	User accuracy (in %)	Commission (%)	Omission (%)
<i>Accuracy assessment</i>				
Limestone	65.56	74.21	25.79	34.44
Sandstone	56.95	65.12	34.88	43.05
Porcellanite	83.78	75.25	24.76	16.17
Calc. shale with Fe concretions	63.91	49.02	50.98	36

Overall accuracy = (107,979/154,971) 69.6769%; Kappa coefficient = 0.5747

Table 4 Data for six sample locations for CaO, MgO, SiO₂ and estimated calcium carbonate (from CaO weight percentage)

Location no.	Measured value of oxides from wet chemical method				CaCO ₃ (Estimated weight using weight of CaO, assuming CaO was fully combined with carbonate)
	SiO ₂	CaO	MgO	Loss of Ignition (LOI)	
1 (Limestone)	12.43	42.56	8.40	33	75.75
2 (Calc. shale)	18.37	38.64	6.60	34.7	68.77
3 (Limestone)	10.86	43.92	5.69	38.64	78.17
4 (Porcellanite)	39.12	30.61	4.21	34.13	54.50
5 (Porcellanite)	38.17	25.28	2.91	31.78	45.50
6 (Sandstone)	46.12	8.65	2.31	41.97	15.39

Values are in weight-percentage

Conclusions

Following conclusions may be drawn from the present study.

1. It has been understood that the spectral maps of Vindhyan rocks (SAM and SID) derived from the processing of ASTER data are comparable with the lithological map derived by conventional method (derived based on field survey with limited modification using satellite image signatures).
2. Both the spectral maps are comparable to each other and are of moderate accuracy in terms of delineation of lithological units. This can be attributed to the fact that the few sedimentary rocks of the area are characterized with limited surface exposures, and are affected with the gradational compositional variations (limestone and calcareous shale). Overall shape of the broad band spectra of these rocks are also close to each other as the rocks are mineralogically similar (e.g. Porcellanite, Calc. shale and limestone all have calcium carbonate with variable concentration).
3. However, SID based lithological map has slightly higher accuracy than the SAM map. This is due to the fact that the probabilistic method like SID takes into account the statistical variability of pixel spectra using statistical divergence while comparing image spectra with the reference end member spectra.
4. Further, accuracy of these spectral maps is also dependent on the details with which the spectral signatures of end members (i.e. spectra of each rock) are recorded in the image (in this case, ASTER image). Accuracy of these spectral maps is also affected by the closeness of diagnostic spectral feature in wavelength domain (i.e. how spectral features are getting overlapped with the spectral feature of other rock within the broad spectral domain of multispectral band of ASTER).

5. Spectral mixing is generally resulted by weathering, gradational variation in composition of each sedimentary unit, extent or size of the rock exposures on the surface. Spectral mixing thought to have contributed in the variation of image spectra of same rock from one place to other. This also have negatively affected the results of spectral mapping algorithms. Spectral mapping algorithm (SID method) suitable to accommodate statistical variation of image spectra using divergence tolerance would provide better accuracy in spectral mapping of rock types.
6. Spectrolithological maps derived using spectral mapping methods correspond well with the discrete geochemical data showing variations of calcium carbonate (roughly estimated from Cao abundance) and silica.

Acknowledgements Authors are grateful to Director, NRSC and Deputy Director, RSAA for their help and guidance. Authors are also grateful to Department of Geology and Mines, Govt. of Jharkhand for sanctioning the fund for field work and satellite data procurement.

References

- Abrams, M. (2000). The Advanced Spaceborne Thermal Emission and Reflection Radiometer (ASTER): Data products for the high spatial resolution imager on NASA's Terra platform. *International Journal of Remote Sensing*, 21(5), 847–859.
- Andrews Deller, M. E. (2006). Facies discrimination in laterites using Landsat Thematic Mapper, ASTER and ALI data examples from Eritrea and Arabia. *International Journal of Remote Sensing*, 27, 5123.
- Azizi, H., Tarverdi, M. A., & Akbarpour, A. (2010). Extraction of hydrothermal alterations from ASTER SWIR data from east Zanjan, northern Iran. *Advances in Space Research*, 46, 99–109.
- Bhan, S. K., & Hegde, V. S. (1985). Targeting areas for mineral exploration—A case study from Orissa, India. *International Journal of Remote Sensing*, 6, 473–479.
- Chabrilat, S., Pinet, P. C., Ceuleneer, G., Johnson, P. E., & Mustard, J. F. (2000). Ronda peridotite massif: Methodology for its geological mapping and lithological discrimination from

- airborne hyperspectral data. *International Journal of Remote Sensing*, 21, 2363–2388.
- Chang, C.-I. (1999). Spectral information divergence for hyperspectral image analysis. In *Geoscience and remote sensing symposium, IGARSS '99 proceedings* (Vol. 1, pp. 501–511).
- Chen, X., Warner, T. A., & Campagna, D. J. (2010). Integrating visible, near-infrared and short-wave infrared hyperspectral and multispectral thermal imagery for geological mapping at Cuprite, Nevada: A rule-based system. *International Journal of Remote Sensing*, 31, 1733–1752.
- Congalton, R. G. (1991). A review of assessing the accuracy of classifications of remotely sensed data. *Remote Sensing of Environment*, 37(1), 35–46.
- Dogan, H. M. (2008). Applications of remote sensing and geographic information systems to assess ferrous minerals and iron oxide of Tokat province in Turkey. *International Journal of Remote Sensing*, 29, 221–233.
- GSI, Unpublished: Geological map in 1:50000 scale for Jharkhand (prepared Toposheet wise).
- Guha, A., Chakraborty, D., Ekka, A. B., Pramanik, K., Vinod Kumar, K., Chatterjee, S., et al. (2012a). Spectroscopic study of rocks of Hutti-Maski schist belt, Karnataka. *Journal of Geological Society of India*, 79, 335–344.
- Guha, A., Rao, A., Ravi, S., Vinod Kumar, K., & Dhananjaya Rao, E. N. (2012b). Analysis of the potentials of kimberlite rock spectra as spectral end member—A case study using kimberlite rock Spectra from the Narayanpet kimberlite Field (NKF), Andhra-pradesh. *Current Science*, 103, 1096–1104.
- Guha, A., Singh, V. K., Parveen, R., Vinod Kumar, K., Jeyaseelan, A. T., & Dhananjaya Rao, E. N. (2013). Analysis of ASTER data for mapping bauxite rich pockets within high altitude lateritic bauxite, Jharkhand, India. *International Journal of Applied Earth Observation and Geoinformation*, 21, 184–194.
- Gürsoy, Ö., & Kaya, Ş. (2017). Detecting of lithological units by using terrestrial spectral data and remote sensing image. *Journal of Indian Society of Remote Sensing*, 45, 259. <https://doi.org/10.1007/s12524-016-0586-1>.
- Hadigheh, S. M. H., & Ranjbar, H. (2013). Lithological mapping in the eastern part of the central Iranian volcanic belt using combined ASTER and IRS data. *Journal of the Indian Society of Remote Sensing*, 41, 921. <https://doi.org/10.1007/s12524-013-0284-1>.
- Hewson, R. D., Cudahy, T. J., Mizuhiko, S., Ueda, K., & Mauger, A. J. (2005). Seamless geological map generation using ASTER in the Broken Hill-Curnamona province of Australia. *Remote Sensing of Environment*, 99, 159–172.
- Hubbard, B. E., & Crowley, J. K. (2005). Mineral mapping on the Chilean “Bolivian Altiplano using co-orbital ALI, ASTER and Hyperion imagery: Data dimensionality issues and solutions. *Remote Sensing of Environment*, 99, 173–186.
- IBM. (2017). Manual of procedure for chemical and instrumental analysis of ores, minerals, ore dressing products and environmental samples. <http://ibm.nic.in/writereaddata/files/08252016122551Manual%20of%20Procedure.pdf>.
- ITT. (2014). ENVI: (Thermal data pre-processing). http://www.exelisvis.com/portals/0/pdfs/envi/Flaash_Module.pdf2009.
- Kalinowski, A., & Oliver, S. A. (2004). ASTER mineral index processing, manual. http://www.ga.gov.au/image_cache/GA7833.pdf.
- Kavak, K. S. (2005). Recognition of gypsum geohorizons in the Sivas Basin (Turkey) using ASTER and Landsat ETM + images. *International Journal of Remote Sensing*, 26, 4583–4596.
- Kruse, F. A., Boardman, J. W., & Huntington, J. F. (2003a). Comparison of airborne hyperspectral data and EO-1 hyperion for mineral mapping. *IEEE Transactions on Geoscience and Remote Sensing*, 41, 1388–1400.
- Kruse, F. A., Boardman, J. W., Huntington, J. F., Mason, P., & Quigley, M. A. (2003b). Evaluation and validation of EO-1 Hyperion for geologic mapping. *IEEE International Geoscience and Remote Sensing Symposium*, 1, 593–595.
- Leverington, D. W. (2010). Discrimination of sedimentary lithologies using Hyperion and Landsat Thematic Mapper data: A case study at Melville Island, Canadian High Arctic. *International Journal of Remote Sensing*, 31, 233–260.
- Mezned, N., Abdeljaoued, S. A., & Boussema, M. R. (2010). A comparative study for unmixing based Landsat ETM + and ASTER image fusion. *International Journal of Applied Earth Observation and Geoinformation*, 12S, S131–S137.
- Milton, E. J., Michael, E. S., Anderson, K., Mathias, K., & Fox, N. (2009). Progress in field spectroscopy. *Remote Sensing of Environment*, 113, 92–109.
- Pour, A. B., & Hashim, S. (2014). ASTER, ALI and Hyperion sensors data for lithological mapping and ore minerals exploration. *Springer Plus*, 3(130), 1–19.
- Rowan, L. C., & Mars, J. C. (2003). Lithologic mapping in the Mountain Pass, California area using advanced spaceborne thermal emission and reflection radiometer (ASTER) data. *Remote Sensing of Environment*, 84, 350–366.
- Rowan, L. C., Schmidt, R. G., & Mars, J. C. (2006). Distribution of hydrothermally altered rocks in the Reko Diq, Pakistan mineralized area based on spectral analysis of ASTER data. *Remote Sensing of Environment*, 104, 74–87.
- Sabins, F. (1999). Remote sensing for mineral exploration. *Ore Geology Reviews*, 14, 157–183.
- San, B. T., & Lutfi Suzen, M. (2011). Evaluation of cross-track illumination in EO-1 Hyperion imagery for lithological mapping. *International Journal of Remote Sensing*, 32, 7872–7889.
- Tangestani, M. H., Jaffari, L., Vincent, R. K., & Sridhar, B. B. M. (2011). Spectral characterization and ASTER-based lithological mapping of an ophiolites complex: A case study from Neyriz ophiolite, SW Iran. *Remote Sensing of Environment*, 115, 2243–2254.
- Tangestani, M. H., & Moore, F. (2000). Iron oxide and hydroxyl enhancement using the Crosta method: A case study from the Zagros Belt, Fars Province, Iran. *Journal of Applied Geoinformation*, 2, 140–146.
- Tommasao, I. D., & Rubinstein, N. (2007). Hydrothermal alteration mapping using ASTER data in the Infiernillo porphyry deposit, Argentina. *Ore Geology Reviews*, 32, 275–290.
- Valdiya, K. S. (2010). *The making of India geodynamic evolution* (1st ed., p. 817). India: Mcmillan.
- Van der Meer, F. D., Van der Werff, H. M. A., Van Ruitenbeek, F. J. A., Hecker, C. A., Bakker, W. H., Noomen, M. F., et al. (2012). Multi- and hyperspectral geologic remote sensing: A review. *International Journal of Applied Earth Observations and Geoinformation*, 14,(1) 112–128.
- White, K., Walden, J., Drake, N., Eckardt, F., & Settlell, J. (1997). Mapping the iron oxide content of dune sands, Namib Sand Sea, Namibia, using Landsat thematic mapper data. *Remote Sensing of Environment*, 62, 30–39.
- Youssef, A. M., Hassan, A. M., & El-Haddad, A. A. A. (2009). Mapping of Prerift—Synrift sedimentary units using enhanced thematic Mapper Plus (ETM +): Sidri—Feiran area, southwestern Sinai Peninsula, Egypt. *Journal of the Indian Society of Remote Sensing*, 37, 377.
- Zhang, X., & Pazner, M. (2007). Comparison of lithologic mapping with ASTER, hyperion, and ETM data in the southeastern Chocolate Mountains, USA. *Photogrammetric Engineering & Remote Sensing*. <https://doi.org/10.14358/pers.73.5.555>.